# Fast Physics-Based Electromigration Analysis for Full-Chip Networks by Efficient Eigenfunction-Based Solution

Xiaoyi Wang<sup>®</sup>, Shaobin Ma, Sheldon X.-D. Tan<sup>®</sup>, Senior Member, IEEE, Chase Cook<sup>®</sup>, Graduate Student Member, IEEE, Liang Chen, Student Member, IEEE, Jianlei Yang<sup>®</sup>, Member, IEEE, and Wenjian Yu<sup>®</sup>, Senior Member, IEEE,

Abstract-Electromigration (EM) becomes one of the most challenging reliability issues for current and future ICs in 10-nm technology and below. In this article, a novel method is proposed for the EM hydrostatic stress analysis on 2-D multibranch interconnect trees, which is the foundation of the EM reliability assessment for large-scale on-chip interconnect networks, such as on-chip power grid networks. The proposed method, which is based on an eigenfunction technique, could efficiently calculate the hydrostatic stress evolution for multibranch interconnect trees stressed with different current densities and nonuniformly distributed thermal effects. The proposed method solves the partial differential equations of transient EM stress more efficiently since it does not require any discretization either spatially or temporally, which is in contrast to numerical methods, such as the finite difference method and finite element method. The accuracy of the proposed transient analysis approach is validated against the analytical solution and commercial tools. The convergence of the proposed method is demonstrated by numerical experiments on practical power/ground networks, showing that only a small number of eigenfunction terms are necessary for the accurate solution. Thanks to its analytical nature, the proposed method is also utilized in efficient EM analysis techniques, such as searching for the void nucleation time by a modified bisection algorithm. The numerical results show that the proposed method is 10X-100X faster than the finite difference method and scales better for larger interconnect trees.

Manuscript received July 26, 2019; revised January 18, 2020 and March 31, 2020; accepted May 25, 2020. Date of publication June 10, 2020; date of current version February 19, 2021. This work was supported in part by the National Natural Science Foundation of China under Grant 61602016, and in part by the Beijing National Research Center for Information Science and Technology under Grant BNR2019ZS01001. This article was recommended by Associate Editor Y. Shi. (Corresponding authors: Xiaoyi Wang; Wenijan Yu.)

Xiaoyi Wang and Shaobin Ma are with the Beijing Engineering Research Center for IoT Software and Systems, Beijing University of Technology, Beijing 100124, China (e-mail: wxy@bjut.edu.cn; mashaobin@emails.bjut.edu.cn).

Sheldon X.-D. Tan, Chase Cook, and Liang Chen are with the Department of Electrical and Computer Engineering, University of California at Riverside, Riverside, CA 92521 USA (e-mail: stan@ee.ucr.edu; ccook009@ucr.edu; lianchen@ucr.edu).

Jianlei Yang is with the School of Computer Science and Engineering, Beijing Advanced Innovation Center for Big Data and Brain Computing, Beihang University, Beijing 100191, China (e-mail: jianlei@buaa.edu.cn).

Wenjian Yu is with the Department of Computer Science and Technology, BNRist, Tsinghua University, Beijing 100084, China (e-mail: yu-wj@tsinghua.edu.cn).

Digital Object Identifier 10.1109/TCAD.2020.3001264

Index Terms—Electromigration (EM), interconnect tree, onchip networks, reliability.

#### I. Introduction

LECTROMIGRATION (EM) reliability is one of the major concerns for the nanometer-integrated chips. The lifetime of the back end of the copper interconnects in nanometer chips are effectively reduced by EM. It is predicted by the international technology roadmap for semiconductors (ITRSs) that the lifetime of wires due to EM will decrease by half for each new technology node. This deterioration of EM reliability is caused by constantly increasing current density and shrinking wire line cross sections as the technology scaling down. EM reliability will become even worse as the technology scales down to 10 nm and below. Although many measures are taken to enhance the EM reliability of copper wire in the manufacturing process, it is also required to consider the challenging EM problem in the design phase, as the verification and optimization of EM lifetime in the design of chips helps to improve the reliability.

Traditionally, Black's equation [1] and Blench limit [2] are employed to predict the mean time to failure (MTTF) due to EM. These methods statistically calculate the MTTF and immortality of the individual branches characterized by current densities and temperature. However, these methods are subject to criticism due to their empirical nature and lack of consideration of residual stress [3], such as thermal and mechanical stress, which can significantly affect the time to failure of the interconnects. Furthermore, these methods are based on the statistical EM time-to-failure data for a single wire. In contrast, the practical on-chip interconnect networks consist of interconnect trees representing continuously connected, highly conductive metal wires within the same level of metalization and terminated by diffusion barriers. Studies show that the stress evolution in each individual wire of a interconnect tree is not independent [4] because the metal atoms migrate across the wire boundaries and EM takes place in the whole interconnect tree [4]. In order to consider these effects, physics-based EM analysis methods for the through silicon via (TSV) [5] and power/ground networks [4], [6], [7] have been proposed. These methods are based on the EM model proposed by Korhonen et al. [8], which model the EM as diffusion-like partial differential equations (PDEs) describing the kinetics of hydrostatic stress evolution on interconnect trees.

0278-0070 © 2020 IEEE. Personal use is permitted, but republication/redistribution requires IEEE permission. See https://www.ieee.org/publications/rights/index.html for more information.

For all those methods based on Korhonen's model, solving the coupled PDEs of hydrostatic stress is a fundamental step. The complexity of the transient solution of hydrostatic stress on the general interconnect tree makes the EM reliability assessment quite a challenging problem. The requirements of accuracy and efficiency to this solution are usually conflicting due to the large size of on-chip interconnect networks. As a result, the existing methods compromise either accuracy or efficiency. In order to ensure the efficiency of the EM analysis for large multibranch interconnect trees, a compact physics-based EM model was proposed by Huang et al. [4] and Sukharev et al. [6]. These methods mainly focus on the steady-state solution of hydrostatic stress instead of transient hydrostatic stress. Thus, these methods cannot provide the accurate time evolution of the hydrostatic stress, which ultimately determines EM failures, such as void nucleation and void growth, for multibranch interconnect trees.

Accurate analytical solutions were also proposed for specific interconnect trees. The first analytical solution was given in the original work of Korhonen et al. [8], describing the hydrostatic stress evolution on a single wire. Although this solution provides insights into the EM, it only works for a single wire, the simplest interconnect structure. Recent studies [9], [10] proposed analytical modeling to provide exact expressions describing the hydrostatic stress evolution in several typical interconnect trees, namely, the straight-line 3-terminal wires, the T-shaped 4-terminal wires, and the cross-shaped 5-terminal wires. Although the proposed model was extended by considering temperature and segment length effects [10], these methods still only work for a few specific wire structures due to the difficulty in obtaining the exact analytical solution. In order to extend the analytical approach to analyze the transient hydrostatic stress evolution for large-scale power/ground networks, Wang et al. [11] proposed a method utilizing the integral transform technique to solve 1-D Korhonen's equations for multisegment wires of a straight metal line, which is a common routing structure of power/ground networks. However, this method still cannot solve the general tree structure of 2-D interconnect trees.

Numerical methods, on the other hand, are usually general enough to provide a numerical solution of transient hydrostatic stress for general interconnect trees, considering the nonuniform residual stress as well as the time-varying thermal and current density effects. However, numerical methods are computationally intensive for full-chip EM analysis. Finite element analysis (FEA)-based method [5] can only solve small structures such as one TSV because of the expensive computational cost. Finite difference methods (FDM) [7], [12] are still too time consuming for full-chip EM reliability assessment. In order to improve the efficiency, Chatterjee et al. [13] proposed a finite difference-based linear time-invariant (LTI) system formulation and reduction of the resulting system matrices to speed up the time-domain simulation based on the matrix exponential method. This method was further improved by Chatterjee et al. [14] using optimized variable-step backward differentiation formulas (BDFs) to solve the LTI system. A Krylov subspace-based reduction technique was applied in the frequency domain to reduce the original system matrices for efficient time-domain solutions and the solution of the finite difference method in the time domain is then accelerated by model order reduction (MOR) [15]. Although accelerated, these finite difference-based methods still require the discretization, both spatially and temporally. The discretization

not only causes numeric errors but also constrains the simulation of hydrostatic stress evolution in a step-by-step manner (usually small steps).

The analytical solutions have advantages over numerical approaches, despite the limited interconnect structure they can solve. Compared to the numerical methods, the advantages of analytical solutions are as follows.

- Korhonen's equations are solved more efficiently since analytical solutions do not require any discretization, which will reduce the number of unknown variables significantly.
- Analytical solutions avoid integrating the transient stress over time with small time steps to get an accurate solution. In contrast, it can compute the stress for a specific time directly.
- 3) Analytical solutions facilitate more efficient EM analysis techniques, such as searching for the void nucleation time by the bisection method or Newton's method [4], which is available only if analytical solutions are provided.

This article proposes a fast physics-based EM analysis method for full-chip EM assessment. By providing an eigenfunction-based solution to the transient hydrostatic stress evolution, the proposed method could check the EM reliability accurately and efficiently. The main contributions of this article are as follows.

- 1) An eigenfunction-based solution is proposed in this article to calculate the transient hydrostatic stress for general 2-D multibranch interconnect trees. It is worth mentioning that previous analytical solutions for single wire [8] and multisegment wire [11] are special cases and could be derived from the proposed solution, which is shown in detail in Section V-B. The proposed method could accommodate both prevoiding and post-voiding boundary conditions and calculate the hydrostatic stress in both phases to reveal the full dynamics of the stress evolution. Moreover, the proposed method could accommodate nonuniform thermal and current effects as well as arbitrary residual stress distribution.
- 2) The convergence of the proposed method is demonstrated by numerical experiments on practical power/ground networks. The experimental results show that only a small number of eigenfunction terms are necessary for sufficient accuracy, despite the conservative large number of eigenfunctions terms used in [11], [16]. As a matter of fact, the convergence of the proposed eigenfunction-based solution is related to the frequency spectrum of the current densities on wires. The numerical experiments on practical power/ground networks show that the convergence of the proposed method is guaranteed due to the limited frequency distribution of the current densities, which has also been argued for the MOR method [15]. Concerning the terms of the model, the proposed method illustrates a similar characteristic to the MOR methods.
- 3) The efficiency of the proposed method is demonstrated by solving large interconnect trees. Due to its low complexity, the proposed method is faster than the numerical methods for large interconnect trees. The experimental results show that the proposed method is 10X–100X faster than the original FDM proposed in [12].
- 4) A modified bisection algorithm based on the proposed semi-analytical solution is proposed to find the

nucleation time  $t_{\text{nuc}}$  quickly for full-chip power/ground networks, which demonstrates that the proposed method can solve the same problems as the numerical methods do, but with the advantage of analytical solutions. Although the numerical methods such as FDM could be accelerated by the MOR method [15], the proposed method has the benefits of an analytical solution. The experimental results on IBM benchmarks show that the proposed method is efficient enough for full-chip EM assessment, without losing accuracy.

The remainder of this article is organized as follows. In Section II, the physics-based model of EM is reviewed, where the structure of the interconnect tree and initial-boundary value problem (IBVP) for EM is illustrated. The skeleton of the eigenfunction-based solution for transient analysis of hydrostatic stress evolution in the void nucleation phase is proposed in Section III. Section IV presents the key techniques to find eigenvalues and eigenfunctions by solving Sturm-Liouville equations. The eigenfunctions-based analytical solution to the transient hydrostatic stress is assembled in Section V. The experimental results are presented in Section VI to show the accuracy, convergence, and efficiency of the proposed method. Finally, we draw the conclusion. Some preliminary results of this article were presented in [16]. We extend it with the second contribution and the fourth contribution, more numerical results and comparisons, and more technical details.

#### II. REVIEW OF PHYSICS-BASED EM MODELING

EM is the migration of metal atoms due to the momentum exchange between electrical field-driven electrons and metal atoms in a metal line. The momentum exchange between atoms and the conducting electrons results in metal depletion at the cathode and a corresponding metal accumulation at the anode ends of the metal wire. When a metal wire is embedded into rigid confinement, which is the case for copper dualdamascene structure, the wire volume changes induced by the atom depletion and accumulation due to migration create tension at the cathode end and compression at the anode end of the wire. The lasting electrical load increases these stresses, as well as the stress gradient along the metal wire. The stress generated inside the embedded metal wire is the prime cause of the void and hillock formation at the opposite ends of the wire. The void nucleation time could be obtained when stress reaches the critical value  $\sigma_{\rm crit}$  and extracted kinetics of the void volume evolution governs the evolution of wire resistance. Degradation of the electrical resistance of the interconnect segment due to the void growth can be derived from the solution of kinetics equation describing the time evolution of stress in the interconnect segments [8], [17]. Since the thin layers of refractive metals form diffusion barriers for copper (Cu) atoms preventing them from diffusion into interlayer (ILD) and intermetal dielectrics (IMDs), as shown by Fig. 1, the EM occurs primarily on the interconnect tree, which is a continuously connected, highly conductive metal with one layer of metalization, terminated by diffusion barriers, as illustrated by Fig. 2. As a general interconnect tree, the wires on the tree could have different widths and different diffusivity caused by nonuniform thermal distribution.

For a single wire segment, the hydrostatic stress evolution  $\sigma(x, t)$  could be described as the diffusion-like equation (1), which was proposed by Korhonen *et al.* [8] to model the void

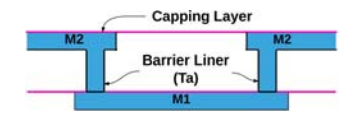


Fig. 1. Layers of Cu interconnects.

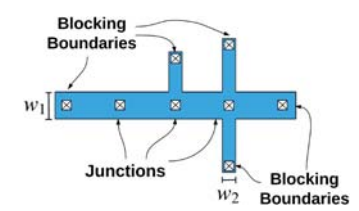


Fig. 2. Interconnect tree structure.

nucleation and kinetics of void size evolution

$$\frac{\partial \sigma(x,t)}{\partial t} = \frac{\partial}{\partial x} \left[ \kappa \left( \frac{\partial \sigma(x,t)}{\partial x} + \mathcal{G} \right) \right] \tag{1}$$

where  $\kappa = [(D_a B \Omega)/(k_B T)]$  is the diffusivity of stress,  $\mathcal{G} = [(Eq^*)/\Omega]$  is the EM driving force, and  $D_a$  is the effective atomic diffusion coefficient, defined as  $D_a = D_0 \exp(-[E_a/k_B T])$ . Here,  $D_0$  is the pre-exponential factor,  $E_a$  is the activation energy, B is the effective bulk elasticity modulus,  $\Omega$  is the atomic lattice volume,  $k_B$  is Boltzmann's constant, T is temperature, E is the electric field,  $q^*$  is the effective charge, x is the coordinate along the wire, and t is time. From Ohm's law, the electric field E could be replaced by the product of resistivity  $\rho$  and current density f, i.e., f is the effective charge f is the elementary charge and f is a known quantity, where f is the elementary charge and f is the effective charge number. As a result, the EM driving force f could be calculated as a function of current density f is the effective charge number.

For an interconnect tree, the hydrostatic stress evolution  $\sigma(x,t)$  could be described by the "extended Korhonen's model" (EKM) proposed in [7] and [13]. In this model, the EM degradation of an interconnect tree is evaluated as a whole because atoms diffuse across branch boundaries at junction nodes on the interconnect tree. For junction nodes on the tree, the boundary conditions (2) represent the facts that the hydrostatic stress should be continuous and the atom flux should be conserved to 0

$$\sigma_{ij_1}(x = x_i, t) = \sigma_{ij_2}(x = x_i, t)$$

$$\sum_{i} w_{ij} J_{a,ij}(x_i, t) = \sum_{i} w_{ij} \kappa_{ij} \left( \frac{\partial \sigma_{ij}}{\partial x} \Big|_{x = x_i} + \mathcal{G}_{ij} \right) = 0 \quad (2)$$

where ij represents the branches connected to junction node i,  $w_{ij}$  is the cross section area of branch ij,  $\kappa_{ij}$  is the diffusivity of branch ij,  $\sigma_{ij}(x,t)$  is stress distribution on branch ij, and  $J_{a,ij}(x,t)$  is the atom flux on branch ij.

For nodes at blocking boundaries of the interconnect tree, the atom diffusion is blocked because the metal lines are confined. Therefore, the atom flux at the block boundary is 0, reflected by the boundary condition

$$J_{a,\ell j}(x_{\ell},t) = \kappa_{\ell j} \left( \frac{\partial \sigma}{\partial x} \bigg|_{x=x_{\ell}} + \mathcal{G}_{\ell j} \right) = 0$$
 (3)

where  $\ell$  is the node at the blocking boundary.

Under the effect of EM-induced driving force, the hydrostatic stress will build up as tensile stress (i.e., positive stress)

or compressive stress (i.e., negative stress). As long as the tensile stress exceeds the critical stress  $\sigma_{\rm crit}$ , the void nucleates. After the void nucleation, the wire comes to the void growth phase, in which the void would enlarge in size as a result of the atom depletion caused by current density. In the void growth phase, the tensile hydrostatic stress on the void nucleation will be effectively released, which usually leads to the hydrostatic stress created in the void nucleation phase release all over the interconnect tree. Besides the change of hydrostatic stress, the wire resistance starts to increase over time in the void growth phase, which usually leads to current density redistribution [18].

From kinetics of the EM-induced void described above, it is clear that the accurate solution to the PDEs (1) is crucial for EM reliability assessment.

## III. TRANSIENT ANALYSIS OF HYDROSTATIC STRESS EVOLUTION IN VOID NUCLEATION PHASE

The hydrostatic stress evolution on a interconnect tree could be described by a group of coupled PDEs, which is a typical IBVP. The proposed method first transforms this IBVP into a homogeneous problem and utilize the "separation of variables" technique to solve it. It then computes the eigenvalues and eigenfunctions numerically. Next, the coefficients of eigenfunctions are determined by initial conditions. Finally, transient hydrostatic stress is calculated as a linear combination of eigenfunctions.

# A. Steady-State Hydrostatic Stress Distribution and Transformation to Homogeneous Transient Problem

To solve coupled Korhonen's equations for the interconnect tree, the governing equation (1), as well as the coupled boundary conditions (2) and (3), should be transformed to homogeneous ones to leverage the use of the separation of variables technique.

Korhonen's equations (1) and boundary conditions (2) and (3) could be transformed into homogeneous ones by subtracting the transient stress distribution  $\sigma(x, t)$  by the steady-state stress distribution  $\sigma(x, \infty)$ . The transformed hydrostatic stress  $\hat{\sigma}(x, t)$  is then defined by

$$\hat{\sigma}(x,t) = \sigma(x,\infty) - \sigma(x,t). \tag{4}$$

To facilitate this transformation, the steady-state hydrostatic stress distribution  $\sigma(x,\infty)$  has to be figured out first. The steady-state stress problem has already been solved in previous works [4], [19]. We hereby shortly review the steady-state stress analysis for convenience. For any branch ij on the interconnect tree, the stress distribution comes to a steady state when it stops changing with time, i.e.,  $([\partial \sigma_{ij}(x,\infty)]/\partial t) = 0$ . Substituting this to Korhonen's equation (1), the atom flux is found to be constant in a steady state and this constant has to be zero according to boundary conditions (3), which is shown by

$$J_{a,ij}(x,\infty) = \kappa_{ij} \left( \frac{\partial \sigma_{ij}(x,\infty)}{\partial x} + \mathcal{G}_{ij} \right) = \text{const} = 0.$$
 (5)

From (5), it is clear that the steady-state stress is linearly distributed on branch ij and satisfies equation (6). In addition, the steady stress is subject to atom conservation equation (7). As a result, the steady-state stress  $\sigma(x, \infty)$  could be solved explicitly from

$$\sigma_{ij}(x_j, \infty) - \sigma_{ij}(x_i, \infty) = l_{ij}\mathcal{G}_{ij}$$
 (6)

$$\sum_{ij} \frac{\sigma_{ij}(x_j, \infty) + \sigma_{ij}(x_i, \infty)}{2} \cdot l_{ij} \cdot w_{ij} = 0.$$
 (7)

Using the transformation equation (4) and zero atom flux equation (5) for steady state, Korhonen's equation is transformed into homogeneous IBVP, which is described by governing equations (8) and boundary conditions

$$\frac{\partial \hat{\sigma}_{ij}(x,t)}{\partial t} = \kappa_{ij} \frac{\partial^2 \hat{\sigma}_{ij}(x,t)}{\partial x^2}$$
 (8)

$$\hat{\sigma}_{ij_1}(x = x_i, t) = \hat{\sigma}_{ij_2}(x = x_i, t)$$

$$\sum_{i} w_{ij} \cdot \kappa_{ij} \frac{\partial \hat{\sigma}_{ij}(x,t)}{\partial x} \bigg|_{x=x_i} \cdot n_i = 0$$
 (9)

$$\kappa_{\ell j} \frac{\partial \hat{\sigma}_{\ell j}(x,t)}{\partial x} \bigg|_{x=x_{\ell}} = 0 \tag{10}$$

where  $n_i$  is the "normal direction" of boundary i on branch ij, which is +1 for right end and -1 for left end of the branch. Meanwhile, the initial conditions are transformed to (11)

$$\hat{\sigma}(x,0) = \sigma(x,\infty) - \sigma(x,0) = \sigma(x,\infty) - \sigma_T \tag{11}$$

where  $\sigma_T$  is the initial residual stress.

#### B. Solving the Transient Problem by Separation of Variables

Since being transformed to homogeneous equations, the initial-boundary value problem (8)–(11) is ready for separation of variables. The solution  $\hat{\sigma}_{ij}(x,t)$  for branch ij of the interconnect tree is assumed to be separated into two parts: 1)  $\psi_{ij}(x)$  and 2)  $\Gamma(t)$ , as shown by

$$\hat{\sigma}_{ii}(x,t) = \psi_{ii}(x) \cdot \Gamma(t). \tag{12}$$

Substituting (12) into (8), the PDEs could be separated into two ordinary differential equations (ODEs) as follows:

$$\frac{\kappa_{ij}}{\psi_{ij}(x)} \frac{\partial^2 \psi_{ij}(x)}{\partial x^2} = \frac{1}{\Gamma(t)} \frac{\partial \Gamma(t)}{\partial t} = -\lambda^2$$
 (13)

where  $\lambda$  is the eigenvalue. Note here that all branches should share the same eigenvalue  $\lambda$ . As a matter of fact, the eigenvalues consist of an infinite series  $0 \le \lambda_1 \le \lambda_2 \le \cdots \le \lambda_m \le \cdots$ . For each eigenvalue, there are two equations to solve: one transient equation (14) with respect to temporal function  $\Gamma(t)$  and another equation (15) with respect to spatial distribution  $\psi_{ij}(x)$ 

$$\frac{d\Gamma(t)}{dt} + \lambda_m^2 \Gamma(t) = 0 \tag{14}$$

$$\frac{\partial^2 \psi_{ij,m}(x)}{\partial x^2} + \frac{\lambda_m^2}{\kappa_{ii}} \psi_{ij,m}(x) = 0.$$
 (15)

The general solutions to (14) and (15) are well known as (16) and (17), respectively

$$\Gamma(t) = C_m \cdot e^{-\lambda_m^2 t} \tag{16}$$

$$\psi_{ij,m}(x) = A_{ij,m} \sin\left(\frac{\lambda_m}{\sqrt{\kappa_{ij}}}x\right) + B_{ij,m} \cos\left(\frac{\lambda_m}{\sqrt{\kappa_{ij}}}x\right). \tag{17}$$

Therefore, the general solution to problem (8) is the linear combination of  $\Gamma(t) \cdot \psi_{ii,m}(x)$ , which is shown by

$$\hat{\sigma}_{ij}(x,t) = \sum_{m=1}^{\infty} C_m e^{-\lambda_m^2 t} \psi_{ij,m}(x)$$
 (18)

where the eigenvalues  $\lambda_m$  and coefficients  $A_{ij,m}$ ,  $B_{ij,m}$ , and  $C_m$  are to be determined by boundary conditions and initial conditions. Finally, the original transient hydrostatic stress  $\sigma(x, t)$  is obtained as (19) as long as the eigenvalues  $\lambda_m$  and eigenvalues  $\psi_m(x)$  being decided

$$\sigma(x,t) = \sigma(x,\infty) - \hat{\sigma}(x,t)$$

$$= \sigma(x,\infty) - \sum_{m=1}^{\infty} C_m e^{-\lambda_m^2 t} \psi_m(x). \tag{19}$$

# IV. SOLVING STURM-LIOUVILLE EQUATIONS FOR EIGENVALUES AND EIGENFUNCTIONS

Equation (15), which decide the eigenvalues and eigenfunctions, are well known as the Sturm-Liouville problem. For branch *ij* on the interconnect tree, the governing equation of the Sturm-Liouville problem could be rewritten as

$$-\frac{\partial^2 \psi_{ij,m}(x)}{\partial x^2} = \omega_{ij,m}^2 \psi_{ij}(x)$$

$$\omega_{ij,m} = \frac{\lambda_m}{\sqrt{\kappa_{ij}}}$$
(20)

where  $\omega_{ij,m}$  is a short notation of frequency on branch ij. Substituting separated solution (12) to boundary conditions (9) and (10), the boundary conditions of the Sturm–Liouville problem could be obtained as

$$\psi_{ij_{1},m}(x=x_{i}) = \psi_{ij_{2},m}(x=x_{i})$$

$$\sum_{i} w_{ij} \cdot \kappa_{ij} \frac{\partial \psi_{ij,m}(x)}{\partial x} \bigg|_{x=x_{i}} \cdot n_{i} = 0$$
(21)

$$\kappa_{j\ell} \frac{\partial \psi_{j\ell,m}(x)}{\partial x} \bigg|_{x=x_{\ell}} = 0 \tag{22}$$

where  $w_{ij}$  is the cross section area of branch ij. These BCs suggest the eigenfunctions  $\psi_m(x)$  should be continuous and obey the Kirchhoff law on interconnect nodes.

In order to obtain the eigenvalues  $\lambda_m$  and eigenfunctions  $\psi_m(x)$ , we have to solve the Sturm–Liouville problem on interconnect trees.

# A. Eigenvalues

The eigenvalues  $\lambda_m$  are key parameters for the solution. However, it is not trivial to determine the eigenvalues for general interconnect trees, in contrast to the simple case of multisegment wires described in [11]. As a matter of fact, the eigenvalues for interconnect trees could only be determined numerically by searching for those eigenvalues satisfying the general solution (17) and boundary conditions (21), (22).

The basic idea is to substitute general solutions (17) to boundary conditions (21), (22) and find the eigenvalues  $\lambda_m$  that result in nontrivial solution of eigenfunctions. Utilizing the fact the eigenfunctions are continuous on boundaries of branch (21), we assume the eigenfunctions' values on the both ends of the branch ij as  $\psi_{i,m} = \psi_{i,m}(x_i)$  and  $\psi_{j,m} = \psi_{j,m}(x_j)$ . Given those values, the coefficients  $A_{ij,m}$  and  $B_{ij,m}$  of the eigenfunction on branch ij is immediately determined by solving the following equations:

$$\psi_{i,m} = A_{ij,m} \sin(\omega_{ij,m} x_i) + B_{ij,m} \cos(\omega_{ij,m} x_i)$$
  
$$\psi_{j,m} = A_{ij,m} \sin(\omega_{ij,m} x_j) + B_{ij,m} \cos(\omega_{ij,m} x_j).$$
(23)

Based on these eigenfunctions, the derivatives on both ends of branch *ij* could be calculated as following equation:

$$\begin{bmatrix} \nabla \psi_{ij,m}(x_i) \\ \nabla \psi_{ij,m}(x_j) \end{bmatrix} = \begin{bmatrix} -\psi'_{ij,m}(x_i) \\ \psi'_{ij,m}(x_j) \end{bmatrix}$$

$$= \begin{bmatrix} \omega_{ij,m} \cot(\omega_{ij,m}l_{ij}) & -\omega_{ij,m} \csc(\omega_{ij,m}l_{ij}) \\ -\omega_{ij,m} \csc(\omega_{ij,m}l_{ij}) & \omega_{ij,m} \cot(\omega_{ij,m}l_{ij}) \end{bmatrix}$$

$$\times \begin{bmatrix} \psi_{i,m} \\ \psi_{j,m} \end{bmatrix}. \tag{24}$$

Equation (24) is called "edge equations," where  $\nabla \psi_{ij,m}(x_i)$  and  $\nabla \psi_{ij,m}(x_j)$  are the inward gradients of eigenfunction  $\psi_{ij,m}(x)$  on branch ends  $x_i$  and  $x_j$ , respectively, and  $l_{ij}$  is the length of branch ij.

Substituting the edge equations (24) to the BCs (21) and (22), the boundary conditions then lead to constraints of the eigenfunction values  $\psi_{i,m}$  on ends of branches, which are represented by

$$K(\lambda_m) \cdot \psi^* = 0 \tag{25}$$

where matrix  $K(\lambda_m)$  consists of combinations of coefficients of edge equations, which depend on eigenvalues  $\lambda_m$ , and  $\psi^* = [\psi_{1,m}, \psi_{2,m}, \dots, \psi_{n,m}]^T$  is the vector of eigenfunction values on nodes of the interconnect tree.

There are nontrivial solutions of eigenfunction that satisfy the boundary conditions only if the determinant of  $K(\lambda_m)$  (K for short) matrix is 0, i.e.,  $\det(K(\lambda_m)) = 0$ , because any K matrix with  $\det(K(\lambda_m)) \neq 0$  implies  $\psi^* = 0$ , which results in a trivial solution of eigenfunction  $\psi_{ij,m}(x) = 0$  for all branch ij. Therefore, those  $\lambda_m$  for which  $\det(K(\lambda_m)) = 0$  are the eigenvalues that result in nontrivial solution of eigenfunction. As a result, the eigenvalues are determined by solving

$$\det(K(\lambda_m)) = 0. \tag{26}$$

Unfortunately, (26) is a complex transcendental equation, which is hard to solve. The elements of K matrix consist of transcendental functions of eigenvalues, such as  $cot(\omega l_{ij})$  and  $csc(\omega l_{ij})$ . Substituting these transcendental functions into a determinant of matrix K makes (26) very hard to solve directly, if not impossible. In order to overcome this difficulty, the Wittrick–Williams algorithm (W-W algorithm) [20] is utilized to search for eigenvalues.

The W-W algorithm is based on the following equation:

$$N(\mu) = \sum_{ij} N_0(\mu) + s(K^{\Delta}(\mu))$$
 (27)

where  $N(\mu)$  is the number of eigenvalues not exceeding  $\mu$ ,  $N_0(\mu)$  is the number of eigenvalues not exceeding  $\mu$  with the Dirichlet boundary conditions,  $K^{\Delta}(\mu)$  is the upper triangular matrix of  $K(\mu)$  matrix using the Gaussian elimination, and  $s(K^{\Delta}(\mu))$  is the number of negative leading diagonal elements of  $K^{\Delta}(\mu)$ . Here,  $N_0(\mu)$  is calculated as the branches are all decoupled by setting the Dirichlet BCs on both ends of the branch.

There are two key numbers to calculate in the W-W algorithm: 1)  $N_0(\mu)$  and 2)  $s(K^{\Delta}(\mu))$ .  $N_0(\mu)$  could be easily calculated by imposing the Dirichlet boundary conditions to both ends of the branch ij, i.e.,  $\psi_{ij}(x=x_i)=\psi_{ij}(x=x_j)=0$ . For each branch ij, the number of eigenvalues in  $[0, \mu]$  under these Dirichlet BCs is calculated by

$$N_0(\mu) = \left| \frac{\omega_{ij} l_{ij}}{\pi} \right| \tag{28}$$

end

where  $\lfloor \cdot \rfloor$  denotes the greatest integer not exceeding the value in the brackets and  $l_{ij}$  is the length of branch ij.

Comparing to calculation of  $N_0(\mu)$ ,  $s(K^{\Delta}(\mu))$  is much harder to compute because the  $K(\mu)$  matrix has to be factorized to its upper triangular matrix  $K^{\Delta}(\mu)$  by the Gaussian elimination. Since the K matrix becomes huge for large interconnect trees, LU factorization of the K matrix could be the bottleneck of the whole W-W algorithm. In order to accelerate the computation of  $s(K^{\Delta}(\mu))$ , we exploit the sparsity of the K matrix. For a interconnect tree with n nodes, the  $K = K(\mu)$  matrix is an  $n \times n$  matrix. However, the nonzero elements of the K matrix are less than  $4 \times n$ . Therefore, the K matrix is a sparse matrix for which the sparse LU factorization methods have been proposed to perform the sparse Gaussian elimination to obtain upper triangular matrix  $K^{\Delta}(\mu)$ . Moreover, the reverse Cuthill–Mckee (RCM) algorithm [21] is utilized to reorder the K matrix so that no fill-ins happens in the sparse LU factorization, which guaranteed the efficiency.

Based on  $N(\mu)$  calculated for any given interval  $[0, \mu]$ , the eigenvalues could easily be confined within intervals by bisection. When the intervals containing the eigenvalues approach to punctuations, the eigenvalues are localized and determined. Instead of some specific eigenvalues, all top M eigenvalues  $\lambda_m$ , m = 1, 2, ..., M are required to solve Korhonen's equations. Therefore, it is inefficient to search for eigenvalues one by one, as the normal bisection method does. In contrast, a customized bisection algorithm (Algorithm 1) is proposed to find all top M eigenvalues in one round, which reduces the unnecessary trial evaluations of  $N(\mu)$  when searching eigenvalues individually. The proposed algorithm (Algorithm 1) includes two stages: the  $\mu$  is exponentially increased in first stage until at least M eigenvalues are included in interval  $[0, \mu]$ . In the second stage, the bisection is utilized to find all the eigenvalues from  $\lambda_1$  to  $\lambda_M$ .

It is worth noticing that there is a trivial eigenvalue  $\lambda_0 = 0$  for BCs (9) and (10) in the void nucleation phase. It is easy to verify that the constant distribution  $\psi_{ij,0}(x) = const$  is the corresponding eigenfunction for this eigenvalue. As a matter of fact, this special eigenvalue implies that the average hydrostatic stress on the interconnect tree remains unchanged in the void nucleation phase.

#### B. Multiplicity of Eigenvalues

For general 2-D interconnect trees, there might be some multifold eigenvalues. In another word, some adjacent eigenvalues are exactly the same. For example, there may exist eigenvalues  $\lambda_{i+1} = \lambda_{i+2} = \cdots = \lambda_{i+k}$ . In this case, the multifold eigenvalue has multiplicity of k.

For an eigenvalue with multiplicity k, there will be k linearindependent eigenfunctions. The multiplicity of eigenvalues
depends on the topology of the interconnect tree. For instance,
it has been proven that all eigenvalues are singlefold (simple) for straight line, illustrated by Fig. 3(a), which is a tree
with special topology. In order to investigate and illustrate the
multiplicity of the eigenvalues, we study some interconnect
trees with typical structures, such as T-shape trees [Fig. 3(b)]
and cross shape trees [Fig. 3(c)] [9].

For example, there are twofold eigenvalues  $(\pi/2l)$ ,  $(3\pi/2l)$ ,  $(5\pi/2l)$ ,  $(7\pi/2l)$ ,  $\cdots$  for the *T*-shape tree illustrated by Fig. 3(b), where l is the branch length. For those twofold eigenvalues  $\lambda_m = ([(2m-1) \cdot \pi]/2l)$ , we could find an eigenfunction  $\psi_{1,2}(x,\lambda_m) = \cos([((2m-1) \cdot \pi)/2l]x)$  on the line

# **Algorithm 1:** Customized Bisection Algorithm to Find All Top M Eigenvalues

```
Input: The number of eigenvalues M to calculate and the accuracy
        requirement \epsilon.
Output: [\lambda_1, \lambda_2, \cdots, \lambda_M]
Initialize the trial eigenvalue \mu to an arbitrary value \lambda_0;
while N(\mu) < M do
Associate the N(\mu) to interval r_0 = ([0, \mu], 0, N(\mu));
Initialize the intervals to check as queue R = \{r_0\};
while R \neq \emptyset do
     Pop the first interval r from R, i.e. r = pop(R);
     Denote r = ([\mu_b, \mu_e], N(\mu_b), N(\mu_e)) where \mu_b is the start point
        and \mu_e is the end point of interval r;
     if N(\mu_b) > M then
          Drop interval r. Continue;
     else if N(\mu_b) = N(\mu_e) then
          Drop interval r. Continue;
     else if \mu_e - \mu_b < \epsilon then
          for i = N(\mu_b) : N(\mu_e) do
               \lambda_i = (\mu_b + \mu_e)/2;
          end
          Finish processing interval r. Continue;
          Calculate N(\mu_m) for middle point \mu_m = (\mu_b + \mu_e)/2 of
          Append both interval r_l = ([\mu_b, \mu_m], N(\mu_b), N(\mu_m)) and
             r_r = ([\mu_m, \mu_e], N(\mu_m), N(\mu_e)) to queue R;
     end
```

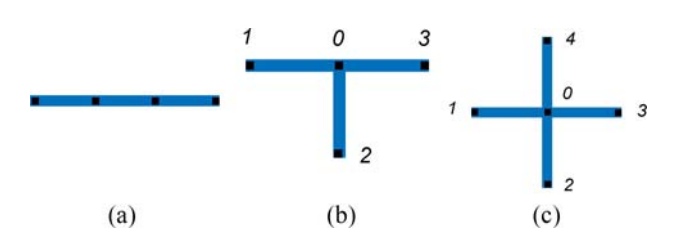


Fig. 3. Interconnect trees with typical structures. (a) Straight line. (b) T-shape. (c) Cross shape.

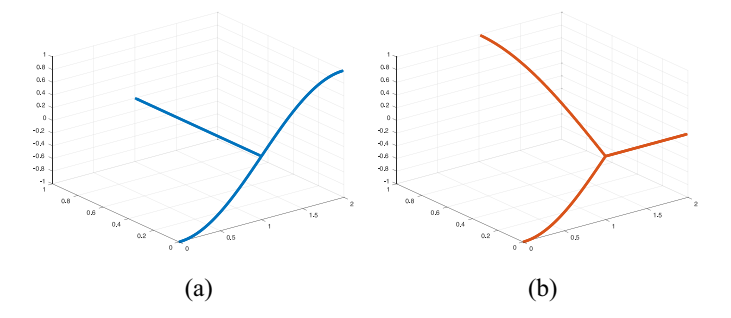


Fig. 4. Eigenfunction  $\psi_{1,3}(x, \lambda_m)$  (a) and  $\psi_{1,2}(x, \lambda_m)$  (b) for eigenvalue  $\lambda_m = (\pi/2l)$  on *T*-shape tree.

1, 0, 2, which has zero value on node 0. Similarly, we can find an eigenfunction  $\psi_{1,3}(x,\lambda_m)=\cos(([(2m-1)\cdot\pi]/2l)x)$  on the line 1, 0, 3. By setting eigenfunction on the other part to 0, we can extend the eigenfunctions to the entire tree, as illustrated by Fig. 4. As we can see from Fig. 4, eigenfunctions  $\psi_{1,2}(x,\lambda_m)$  and  $\psi_{1,3}(x,\lambda_m)$  are linearly independent since  $\psi_{1,2}(x,\lambda_m)\neq 0$ ,  $\psi_{1,3}(x,\lambda_m)=0$  on branch 0, 2 and  $\psi_{1,2}(x,\lambda_m)=0$ ,  $\psi_{1,3}(x,\lambda_m)\neq 0$  on branch 0, 3. Although linearly independent, these two eigenfunctions are not orthogonal to each other, i.e.,  $\int_T \psi_{1,2} \cdot \psi_{1,3} \neq 0$ .

Note that having multifold eigenvalues for some interconnect trees does not mean all eigenvalues are multifold on this tree. The eigenvalues of T-shape tree with Neumann's BCs are actually  $(\pi/2l)$ ,  $(\pi/l)$ ,  $(3\pi/2l)$ ,  $(2\pi/l)$ ,  $(5\pi/2l)$ ,  $(3\pi/l)$ ,  $(7\pi/2l)$ , ..., with twofold and singlefold eigenvalues interleaving with each other. For the cross-shape tree as illustrated by Fig. 3(c), we could find threefold eigenvalues using the same approach described above. Here, we illustrate and analyze the multiplicity of the eigenvalues by constructing analytical eigenfunctions. However, the multiplicity of eigenvalues for general interconnect trees are certainly depending on the topology and parameters of the tree. Therefore, the corresponding eigenfunctions should be calculated numerically instead. See Section IV-C for this.

Despite the multiplicity of the eigenvalues, the proposed algorithm (Algorithm 1) could still be utilized to find all of the eigenvalues. In practice, the multifold eigenvalues could be detected in an arbitrarily short interval containing more than one eigenvalues. In this process, Algorithm 1 shows its stability concerning numerical truncation errors.

Although the eigenfunctions for multifold eigenvalues could not be solved analytically for a general interconnect tree, investigations to the linear-independent eigenfunctions in this section could enlighten the numerical solution of the orthonormal eigenfunctions corresponding to multifold eigenvalues for interconnect trees.

## C. Eigenfunctions

Once the eigenvalues are figured out, the corresponding eigenfunctions could be then calculated by solving PDEs (20) with given  $\lambda_m$ . The general solution  $\psi_{ij}(x)$  on branch ij to the PDE is given by (23). The unknown  $A_{ij}$  and  $B_{ij}$  could be obtained by solving (29) if the eigenfunction values on each end of the branch are known

$$\begin{bmatrix} \psi_{ij,m}(x_i) \\ \psi_{ij,m}(x_j) \end{bmatrix} = \begin{bmatrix} \sin(\omega_{ij,m}x_i) \cos(\omega_{ij,m}x_i) \\ \sin(\omega_{ij,m}x_j) \cos(\omega_{ij,m}x_j) \end{bmatrix} \begin{bmatrix} A_{ij} \\ B_{ij} \end{bmatrix}. \quad (29)$$

Substituting the eigenfunction values  $\psi_{i,m} = \psi_{ij,m}(x_i)$  on node i and  $\psi_{j,m} = \psi_{ij,m}(x_j)$  on node j to (29), the eigenfunction  $\psi_{ij,m}(x)$  on branch ij could be represented as

$$\psi_{ij,m}(x) = \psi_{i,m} \frac{\sin(\omega_{ij,m}(x_j - x))}{\sin(\omega_{ij,m}l_{ij})} + \psi_{j,m} \frac{\sin(\omega_{ij,m}(x - x_i))}{\sin(\omega_{ij,m}l_{ij})}.$$
(30)

As a result, the task to calculate eigenfunctions  $\psi_{ij,m}(x)$  is equivalent to calculating eigenfunction values  $\psi^* = [\psi_{1,m}, \psi_{2,m}, \dots, \psi_{n,m}]^T$  on each node of the interconnect tree.

The eigenfunction values  $\psi^*$  on nodes of the tree could be solved from linear equations (25). Because  $\det(K(\lambda_m)) = 0$ , the eigenfunction values  $\psi^*$  on nodes could only be uniquely determined with respect to some prescribed elements. In contrast to the method proposed in [16], the multiplicity of the eigenvalues and eigenfunctions is considered here, which indicates there could be multiple linear-independent  $\psi^*$  obtained by solving equation (25). Without losing generality, we assume that eigenvalue  $\lambda_m$  has multiplicity of k, ( $k = 1, 2, \ldots$ ). From following Theorem 1, we expect exactly k nonzero solutions for equation  $K(\lambda_m) \cdot \psi^* = 0$  since there are k linear-independent eigenfunctions for eigenvalue  $\lambda_m$ .

Theorem 1: The eigenfunctions  $\psi_1(x), \psi_2(x), \dots, \psi_k(x)$  are linearly independent if and only if  $\psi_1^*, \psi_2^*, \dots, \psi_k^*$  are

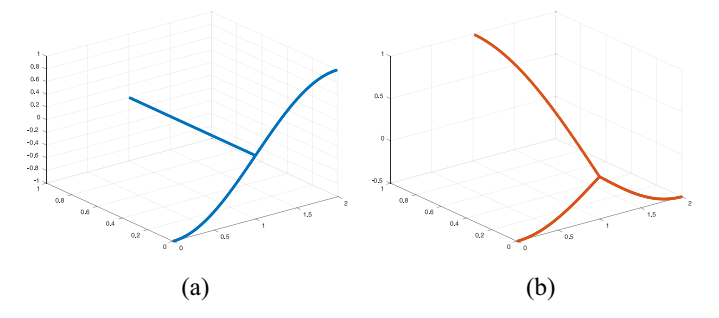


Fig. 5. Eigenfunction (a) and the orthogonalized eigenfunction (b) for eigenvalue  $\lambda_m = (\pi/2l)$  on T-shape tree.

linearly independent, where  $\psi_i^*$  is the vector of eigenfunction  $\psi_i(x)$ 's values on nodes of the tree (i = 1, 2, ..., k).

Therefore, the rank of nullspace of  $K(\lambda_m)$  is k and the basis of its nullspace is the nontrivial solution of  $K(\lambda_m) \cdot \psi^* = 0$ . In order to find the nullspace of  $K(\lambda_m)$  stably, a sparse QR factorization method proposed in [22] is used as the following equation:

$$K(\lambda_m) = K_Q \cdot K_R. \tag{31}$$

There are k zero diagonal elements in upper triangular matrix  $K_R$  and the corresponding column vectors of  $K_Q$  form the basis of the nullspace of  $K(\lambda_m)$ . Therefore, those column vectors of  $K_Q$  are the nonzero solutions  $\psi_i^*$  ( $i=1,\ldots,k$ ) for  $K(\lambda_m)\cdot\psi^*=0$ . Substituting these  $\psi_i^*$  to (30), the eigenfunctions for eigenvalue  $\lambda_m$  are determined.

Since  $K_Q$  is an orthogonal matrix from the QR factorization, solutions  $\psi_i^*$   $(i=1,\ldots,k)$  are orthogonal to each other. However, the eigenfunctions corresponding to  $\psi_i^*$  are not orthogonal to each other. This fact could be illustrated by the linear-independent eigenfunctions for eigenvalue  $(\pi/2l)$  on the T-shape tree shown by Fig. 4. The inner product of these eigenfunctions is not zero, which indicates the eigenfunctions are not orthogonal to each other.

Nevertheless, the orthogonal eigenfunctions are desired because it is easier to represent other solution functions by the orthogonal eigenfunctions. Therefore, the modified Gram–Schmidt process is utilized to orthogonalize the linear-independent eigenfunctions for the same multifold eigenvalue. For example, orthogonalized eigenfunctions for the *T*-shape interconnect tree are shown in Fig. 5.

For those eigenfunctions corresponding to different eigenvalues, it has already been proven that the eigenfunctions for different eigenvalues are orthogonal to each other. Therefore, eigenfunctions  $\psi_m(x)$ ,  $m=1,2,\ldots$ , calculated by the proposed method are orthonormal basic solutions of the Sturm-Liouville equations (20).

## V. SEMI-ANALYTICAL SOLUTION OF THE TRANSIENT HYDROSTATIC STRESS

Although the eigenvalues and eigenfunctions are calculated numerically as shown in the previous section, the transient hydrostatic stress could be represented by an analytical solution in terms of eigenvalues and eigenfunctions.

#### A. Coefficients of Basic Solution to Satisfy Initial Conditions

Since the eigenvalues  $\lambda_m$  and eigenfunctions  $\psi_m(x)$  are determined, the solution (18) as a linear combination of basic

solutions  $\Gamma(t) \cdot \psi_{ij,m}(x)$  are to be specified in terms of the coefficients  $C_m$ . The coefficients  $C_m$  would be solved by setting the solution (18) to satisfy the initial conditions, as shown by

$$\hat{\sigma}_0(x) = \hat{\sigma}(x, t = 0) = \sum_{m=1}^{\infty} C_m \psi_{ij,m}(x).$$
 (32)

Since the eigenfunctions are orthogonal to each other, which means inner product of eigenfunctions  $\langle \psi_{m_1}(x) \cdot \psi_{m_2}(x) \rangle = \sum_{ij} w_{ij} \int_{x_i}^{x_j} \psi_{ij,m_1}(x) \cdot \psi_{ij,m_2}(x) dx = 0$  for eigenvalues  $\lambda_{m_1} \neq \lambda_{m_2}$ , the coefficients  $C_m$  could be obtained by calculating the inner product of each eigenfunctions  $\psi_m(x)$  to the initial conditions  $\hat{\sigma}_0(x)$ , as shown by

$$C_m = \frac{\langle \psi_m(x) \cdot \hat{\sigma}_0(x) \rangle}{\langle \psi_m(x) \cdot \psi_m(x) \rangle} = \frac{\sum_{ij} w_{ij} \int_{x_i}^{x_j} \psi_{ij,m}(x) \cdot \hat{\sigma}_0(x) dx}{\sum_{ij} w_{ij} \int_{x_i}^{x_j} \psi_{ij,m}^2(x) dx}. \tag{33}$$

Here, the norm of eigenfunctions  $\langle \psi_m(x) \cdot \psi_m(x) \rangle$  could be calculated analytically as the following equation:

$$\langle \psi_{m}(x) \cdot \psi_{m}(x) \rangle$$

$$= \sum_{ij} w_{ij} \int_{x_{i}}^{x_{j}} \psi_{ij,m}^{2}(x) dx = \sum_{ij} w_{ij}$$

$$\times \left( \frac{\left(\psi_{i,m}^{*2} + \psi_{j,m}^{*2}\right)}{\sin^{2}(\omega_{ij,m}l_{ij})\omega_{ij,m}} \left[ \frac{\omega_{ij,m}l_{ij} - \sin(\omega_{ij,m}l_{ij})\cos(\omega_{ij,m}l_{ij})}{2} \right] + \frac{\psi_{i,m}^{*}\psi_{j,m}^{*}}{\sin^{2}(\omega_{ij,m}l_{ij})\omega_{ij,m}} \left[ \sin(\omega_{ij,m}l_{ij}) - \omega_{ij,m}l_{ij}\cos(\omega_{ij,m}l_{ij}) \right]. \tag{34}$$

Generally the inner product of eigenfunctions and initial stress distribution  $\langle \psi_m(x) \cdot \hat{\sigma}_0(x) \rangle$  could be calculated numerically by the fast Fourier transform. However, if a stress distribution f(x) on the interconnect tree is a piecewise linear (PWL) function that satisfies the boundary conditions, then its inner product to eigenfunctions could be computed as (35). Note that the initial stress distribution  $\hat{\sigma}_0(x) = \sigma(x, \infty) - \sigma_T$  happens to be such a PWL function. Therefore, the inner product of eigenfunctions and initial stress distribution could also be calculated analytically

$$\langle \psi_{m}(x) \cdot f(x) \rangle = \sum_{ij} -\frac{w_{ij}}{\omega_{ij,m}^{2} l_{ij}} \left( \left[ f_{ij}(x_{j}) - f_{ij}(x_{i}) \right] \times \left[ \psi_{ij,m}(x_{i}) - \psi_{ij,m}(x_{j}) \right] \right).$$

$$(35)$$

### B. Special Cases of Analytical Hydrostatic Stress Solution

Although parameters  $\lambda_m$  and  $\psi_m(x)$  are decided numerically, the proposed eigenfunction-based solution still has characteristics of analytical solution. In some special cases, where the eigenvalues and eigenfunctions are known analytically, such as a single wire [8] and multisegment wire [11], the proposed method becomes natural to the known analytical solutions.

For the single wire case, the eigenvalues and eigenfunction with Neumann's BCs (i.e., BCs in the void nucleation phase) are already known as

$$\omega_m = \frac{\lambda_m}{\sqrt{\kappa}} = \frac{m\pi}{l}, \quad m = 0, 1, 2, \dots$$

$$\psi_m(x) = \cos(\omega_m x) = \cos\left(\frac{m\pi}{l}x\right) \tag{36}$$

and the closed form expression of hydrostatic stress given by [8] is known as

$$\sigma(x,t) = \sigma_T + \mathcal{G}l \left\{ \frac{1}{2} - \frac{x}{l} - 4 \sum_{n=0}^{\infty} \frac{\cos\left(\frac{(2n+1)\pi}{l}x\right)}{(2n+1)^2 \pi^2} e^{-\kappa \frac{(2n+1)^2 \pi^2}{l^2}t} \right\}$$
(37)

where l is the length of wire and  $\sigma_T$  is the initial residual stress. The analytical solution of transient stress could also be transformed to summation of series as the following equation:

$$\hat{\sigma}(x,t) = \sigma(x,\infty) - \sigma(x,t) = \sum_{n=0}^{\infty} \frac{4\mathcal{G}l}{(2n+1)^2 \pi^2} \cos\left(\frac{(2n+1)\pi x}{l}\right) e^{-\kappa \frac{(2n+1)^2 \pi^2}{l^2}t} = \sum_{m=1}^{\infty} C_m \psi_m(x) e^{-\lambda_m^2 t}$$
(38)

where steady-state stress  $\sigma(x, \infty) = \sigma_T + \mathcal{G}l([1/2] - [x/l])$  is a linear function along the wire.

It could be proven that the proposed method results in exactly the same transient solution by showing that the same eigenvalues  $\omega_m$ , eigenfunctions  $\psi_m(x)$ , and coefficients  $C_m$  could be obtained by the proposed method. From (23), the eigenfunction values on each end of the wire is obtained as

$$\begin{bmatrix} \psi_{0,m} \\ \psi_{l,m} \end{bmatrix} = \begin{bmatrix} \sin(\omega_m 0) & \cos(\omega_m 0) \\ \sin(\omega_m l) & \cos(\omega_m l) \end{bmatrix} \begin{bmatrix} A \\ B \end{bmatrix} = K_1 \cdot \begin{bmatrix} A \\ B \end{bmatrix} (39)$$

where  $\psi_{0,m} = \psi_m(x=0)$ ,  $\psi_{l,m} = \psi_m(x=l)$ , and matrix  $K_1 = \begin{bmatrix} 0 & 1 \\ \sin(\omega_m l) & \cos(\omega_m l) \end{bmatrix}$ . The gradients on each end of the wire are obtained as (40) by taking the derivatives

$$\begin{bmatrix} \nabla \psi_{0,m} \\ \nabla \psi_{l,m} \end{bmatrix} = \omega_m \begin{bmatrix} -\cos(\omega_m 0) & \sin(\omega_m 0) \\ \cos(\omega_m l) & -\sin(\omega_m l) \end{bmatrix} = K_2 \cdot \begin{bmatrix} A \\ B \end{bmatrix}$$
(40)

where matrix  $K_2 = \omega_m \begin{bmatrix} -1 & 0 \\ \cos(\omega_m l) & -\sin(\omega_m l) \end{bmatrix}$ . From (40), it could be seen that the nontrivial eigenfunction exists (i.e.,  $A \neq 0$  or  $B \neq 0$ ) iff.  $det(K_2) = 0$ . Calculating  $det(K_2) = \omega_m \sin(\omega_m l)$ , it is clear that the eigenvalue is either  $\omega_0 = 0$  or  $\omega_m = (m\pi/l)$ , which agrees with the known eigenvalues. Let us also show how the W-W algorithm is applied to figure out the eigenvalues numerically in this case. For any trial value  $\mu$  that  $\sin(\mu l) \neq 0$ , the  $K(\mu)$  matrix could be built by (24) as follows:

$$K(\mu) = \mu \begin{bmatrix} \cot(\mu l) & -\csc(\mu l) \\ -\csc(\mu l) & \cot(\mu l) \end{bmatrix}. \tag{41}$$

Factorizing the  $K(\mu)$  matrix manually by LU, the upper triangular matrix  $K^{\Delta}(\mu)$  is obtained as the following equation:

$$K^{\Delta}(\mu) = \mu \begin{bmatrix} \cot(\mu l) & -\csc(\mu l) \\ 0 & -\tan(\mu l) \end{bmatrix}. \tag{42}$$

Note that  $\cot(\mu l)$  and  $\tan(\mu l)$  must have the same sign. Therefore, sign count  $s(K^{\Delta}(\mu)) = 1$  and eigenvalue number in  $[0, \mu]$  is  $N(\mu) = \lfloor \mu l/\pi \rfloor + 1$ , which implies eigenvalues as  $\omega_m = (m\pi/l)$  plus one zero eigenvalue  $\omega_0 = 0$ .

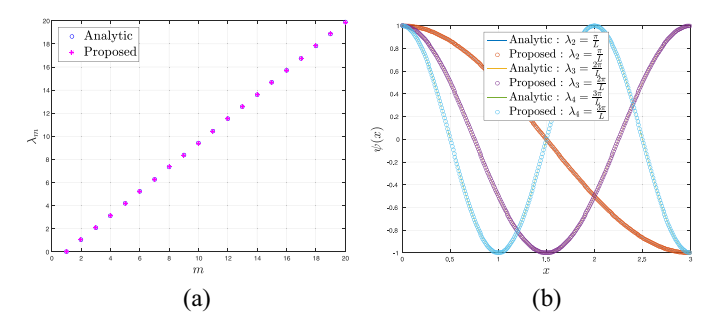


Fig. 6. (a) Eigenvalues  $\lambda_m$  and (b) eigenfunctions  $\psi(x)$  for a single wire with length L=1.

To figure out the eigenfunctions, the eigenvalues  $\omega_m = (m\pi/l)$  and Neumann's BCs could be substituted to (40) and it is clear that A=0 and B=1 is the normalized solution. Therefore, eigenfunctions are  $\psi_m(x) = \cos(\omega_m x) = \cos([m\pi/l]x)$ , which also agree with the known analytical eigenfunctions.

The coefficients  $C_m$  could be figured out from the Fourier series of the transformed initial condition  $\hat{\sigma}_0(x) = \sigma(x, \infty) - \sigma_T = \mathcal{G}L([1/2] - [x/l])$ , shown by the following equation:

$$\hat{\sigma}_0(x) = \sum_{n=0}^{\infty} \frac{4\mathcal{G}L}{(2n+1)^2 \pi^2} \psi_{2n+1}(x). \tag{43}$$

Therefore, the coefficients  $C_m$  are calculated as follows:

$$C_m = \begin{cases} 4\mathcal{G}L/(m^2\pi^2), & m = 2n+1\\ 0, & m = 2n \end{cases}$$
 (44)

which are eaxctly the same as those in the known analytical solution (36).

The numerical results of eigenvalues and eigenfunctions are shown in Fig. 6(a) and (b). Compared to the analytical solution, the numerical solution given by the proposed method is quite accurate, with a relative error less than  $10^{-6}$ . The numerical results also show that the W-W algorithm is quite robust despite the K matrix becomes almost singular when  $\mu$  approaches  $\omega_m$ .

For the multisegment case in [11], the eigenvalues and eigenfunctions are the same as those of the single wire because the segments are assumed to have identical width and diffusivity  $\kappa$ . The main difference is the steady-state stress is a piecewise linear function distributed on the segments instead of a simple linear function for the single wire. The integrated transform technique proposed in [11] leads to exactly the same  $C_m$  when the  $C_m$  is calculated by (35) and (34) to satisfy the piecewise linear-distributed ICs. As a result, the proposed method is equivalent to the integrated transform-based method [11] in the special case of a multisegment wire.

# C. Nonuniform Current Density, Nonuniform Thermal Effect, and Nonideal Rectangular Wires Due to Lithography

The proposed method is able to accommodate the nonuniform current density and thermal effect. The nonuniform current density situation is illustrated by Fig. 7(a). The current densities on the left and right branches are different because of the different wire widths. This case has already been handled in (21) and (33) by considering different wire width  $w_{ij}$ . The nonuniform thermal distribution situation is illustrated by

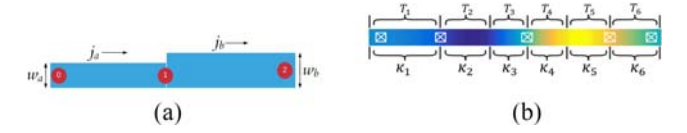


Fig. 7. (a) Nonuniform current densities. (b) Nonuniform thermal distribution.



Fig. 8. Wires with irregular shape due to the lithography process [23]. (a) Short wire. (b) Long wire.

Fig. 7(b). In order to find out the transient hydrostatic stress in this case, one idea is to divide the wire into segments so that each segment has the same temperature. Because the diffusivity  $\kappa$  is a function of the temperature T, each segment on the wire has varying diffusivity  $\kappa_{ij}$ . This case has already been handled in the proposed method by considering the nonuniform diffusivity  $\kappa_{ij}$ .

Due to the lithography process, the fabricated wires do not have the ideal 2-D rectangular shapes, as illustrated in Fig. 8. The proposed method is not able to precisely solve the hydrostatic stress for those irregular wires. To mitigate this problem, one idea is to approximate the current densities on irregular wires. Note that the irregularity occurs mainly on ends of the wire and it causes larger distortion on short wires than on long wires, as shown in Fig. 8. In order to calculate the stress on short wires by the proposed method, the wire is divided into different regions to approximate the current densities in irregular-shaped regions [see Fig. 8(a)]. The average current densities in each region are used as the approximation. As a result, the corrected current densities  $j_1$  and  $j_3$  in Fig. 8(a) become larger than  $j_2$  because lithography variations narrow down the wire at the ends. After the current density correction, the proposed method can be utilized to solve the stress distribution. For the long wire, the proposed method can be applied directly to calculate the hydrostatic stress because the shape variations have a little impact on the stress distribution.

It is noticed in [19] that the current crowding effect also has a less significant impact on longer wires, which confirms that it is reasonable to approximate hydrostatic stress with the proposed method for long wires. For the shorter wires that have totally different shapes from rectangle due to lithography, a new model is required to accurately calculate the hydrostatic stress, which will be studied in the future. It is also worth noticing that short wire is less concerned for EM because of the Blench limit effects [19].

## VI. NUMERICAL RESULTS AND DISCUSSION

# A. Accuracy of the Eigenfunction-Based Transient Hydrostatic Stress Analysis Method

In order to validate the accuracy of the proposed method, the experimental results of transient hydrostatic stress evolution in the void nucleation phase are compared with the analytical solutions in [9]. Since only typical interconnect structures, including three terminals, four terminals, and five terminal junctions are analyzed in [9], we compare the transient solutions of the proposed method to those from [9] for these wire

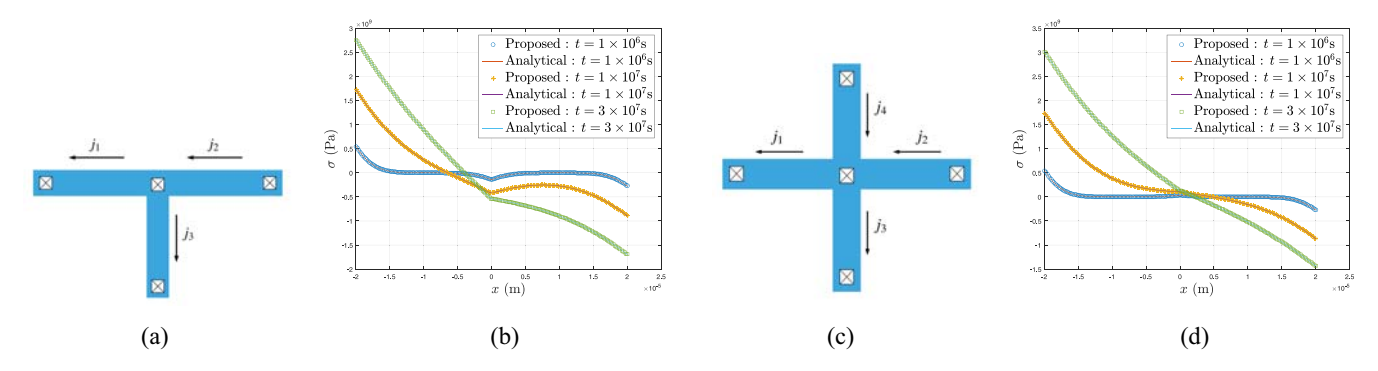


Fig. 9. (a) *T*-shape interconnect tree with branch length  $2 \times 10^{-5}$  m and current densities  $j_1 = 4 \times 10^{10}$  A/m²,  $j_2 = 2 \times 10^{10}$  A/m², and  $j_3 = 1 \times 10^{10}$  A/m² and (b) hydrostatic stress evolution on it. (c) Cross-shape interconnect tree with branch length  $2 \times 10^{-5}$  m and current densities  $j_1 = 4 \times 10^{10}$  A/m²,  $j_2 = 2 \times 10^{10}$  A/m²,  $j_3 = -2 \times 10^{10}$  A/m², and  $j_4 = 1 \times 10^{10}$  A/m² and (d) hydrostatic stress evolution on it.

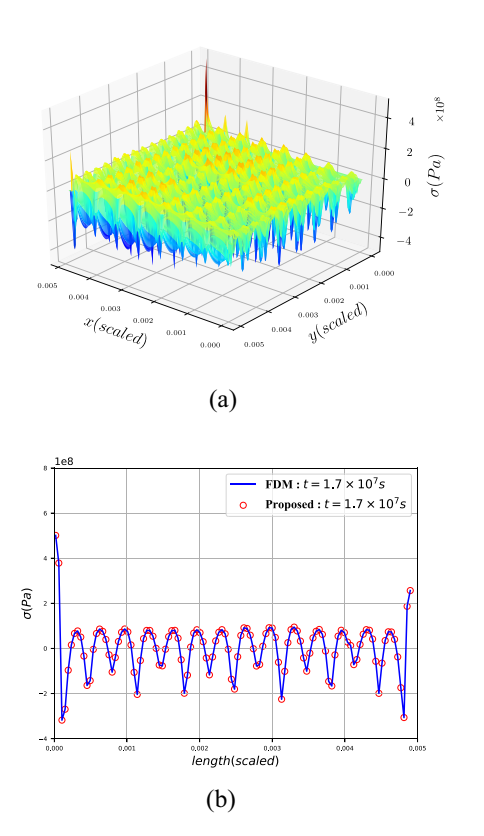


Fig. 10. (a) Transient hydrostatic stress on layer 3 of IBMPG2 at time  $t = 1.7 \times 10^7$  s and (b) transient hydrostatic stress of a specific interconnect tree on this layer calculated by the proposed method.

structures. Fig. 9 shows the structures of interconnect, current density, and the transient hydrostatic stress evolution in the void nucleation phase.

In both cases, the proposed method is accurate enough compared to the results of the analytical solution or COMSOL simulation, with max error 0.2%. As a matter of fact, the accuracy of the proposed method depends on the number of eigenfunctions used to represent the transient solution. The more eigenfunctions used, the more accurate the solution is. The sufficient number of eigenfunctions depends on the spatial variance of current density. This topic will be discussed in Section VI-B.

Note that our method could compute transient stress evolution for arbitrarily complex interconnect trees beyond these typical structures. In order to demonstrate this, the transient stress for the benchmark IBMPG2 [24] is calculated by the proposed method. The transient stress on layer 3 at time  $t = 1.7 \times 10^7$  s is shown in Fig. 10(a). The transient stress on a specific interconnect tree on this layer is also shown in Fig. 10(b), where the results of FDM and our method are illustrated.

In order to evaluate the approximation of stress on the wires with irregular shape due to the lithography process, the experimental results of transient and steady hydrostatic stress for a short irregular wire, shown in Fig. 8(a), and long irregular wire, shown in Fig. 8(b), are compared in Fig. 11. COMSOL is used to model and solve the hydrostatic stress on the irregular wires. For the short irregular wire, the stress distributions are reasonably approximated by the proposed method with current density correction, shown by "proposed w/*j* correction" plot in Fig. 11(a). The average relative error of stress distributions on the short wire is 9.4%. For the long irregular wire, the stress distributions are properly approximated by the proposed method, even without correcting the current densities, shown by "proposed w/o *j* correction" plot in Fig. 11(b). The average relative error of stress distributions on the long wire is 7.0%.

# B. Convergency of the Eigenfunction-Based Transient Hydrostatic Stress Analysis Method

Although the transient stress solution is theoretically an infinite series as shown by (18), only the first M items are used in practice to compute the solution as long as it is accurate enough. Despite the quite conservative M=200 is adopted in previous works [11], [16], the item number M is not necessarily large. In fact, the experiments on practical interconnect trees in IBM power/ground benchmarks show that the item number around 20–30 is enough for an accurate solution. The appropriate item number M is determined by frequency domain analysis as follows.

Since the transient stress solution is a linear combination of eigenfunctions  $\psi_m(x)$  with coefficients  $C_m$ , small coefficients with little effect could be truncated out. From (32) and (11), we can see the coefficients  $C_m$  are decided by the frequency distribution of the steady-state stress  $\sigma(x, \infty)$ . Therefore, the frequency spectrum of the steady-state stress is analyzed to understand how many eigenfunctions are necessary for enough accuracy. The steady-state stress and its frequency spectrum on an interconnect of the IBMPG4 benchmark are shown in Fig. 12. This interconnect tree has 174 branches and the steady-state stress  $\sigma(x, \infty)$  is calculated according to the

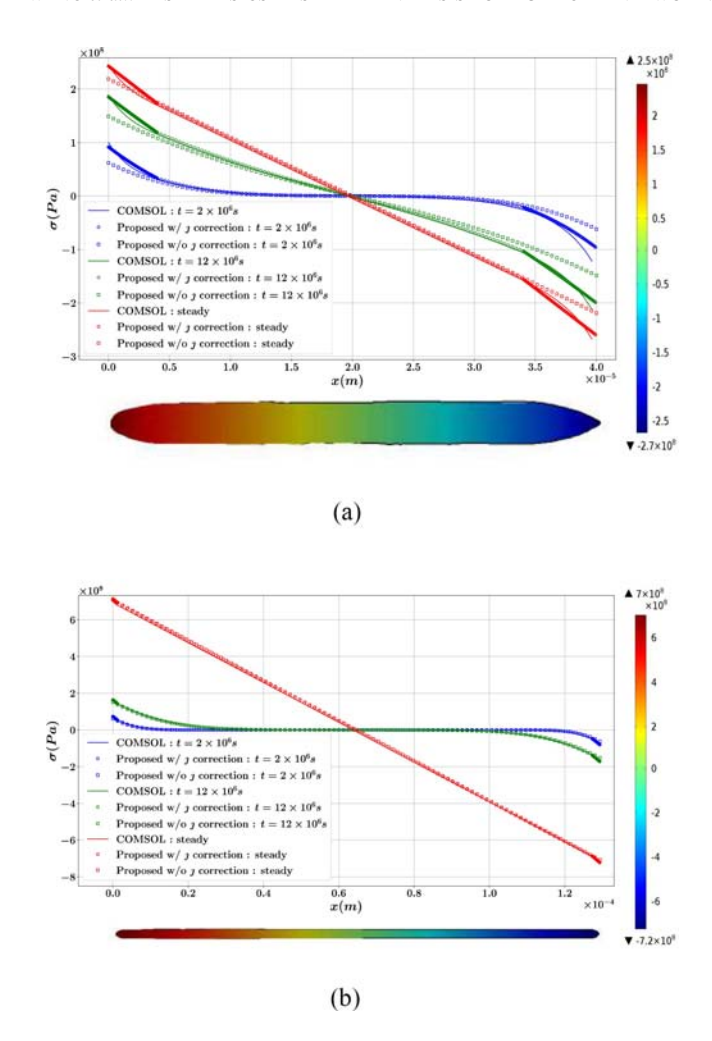
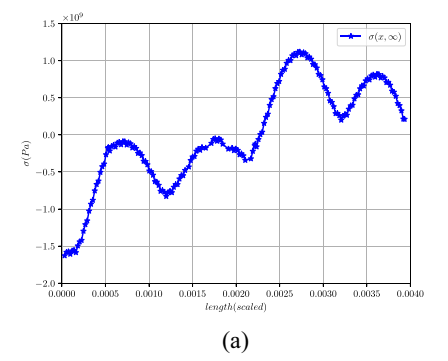


Fig. 11. Hydrostatic stress on: (a) short irregular wire and (b) long irregular wire.

voltage distribution as shown in [19]. Although the accurate solution could be guaranteed with eigenfunction number M=174, the frequency spectrum of  $\sigma(x,\infty)$  in Fig. 12(b) shows M = 20-30 is enough to capture the major components of the eigenfunction. In order to prove this, a different number of eigenfunctions are used to represent the steady-state stress on the interconnect of the IBMPG4 benchmark. Fig. 13(a) shows the representation of steady-state stress with M = 5, 10, 25 eigenfunctions. As we can see, the eigenfunctionbased solution converges quickly. With M=25, the error to exact stress decreases to 3.72%. Correspondingly, the transient stress calculated by 25 eigenfunctions is also good enough. Fig. 13(b) shows the transient stress  $\sigma(x, t)$  at  $t = 1 \times 10^{13}$ calculated by M = 25 eigenfunctions. As we can see, the transient solution calculated by 25 eigenfunctions agrees well with the result of FDM.

# C. Efficiency of the Eigenfunction-Based Transient Hydrostatic Stress Analysis Method

In order to demonstrate the efficiency of the proposed method, a multibranch interconnect tree of n consecutive T-junctions is proposed as the test case for performance, as shown by Fig. 14. Note that there are 2n+1 branches on the testing interconnect trees. We then compare the performance of the proposed method and FDM [12] with an increasing number of n to show the efficiency. The proposed method and



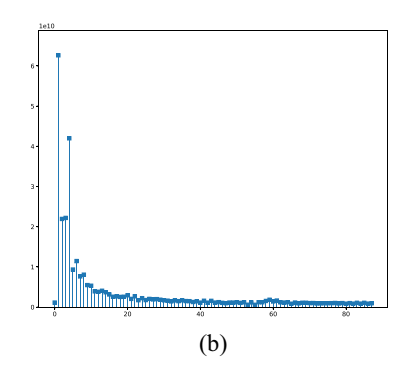
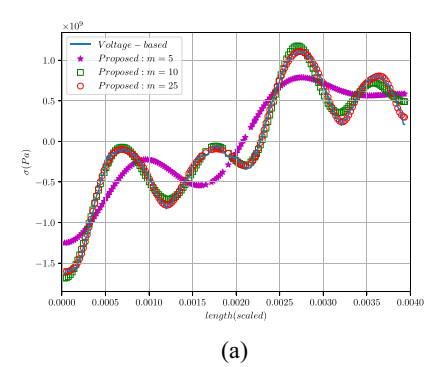


Fig. 12. (a) Steady-state stress  $\sigma(x,\infty)$  and (b) its frequency specturm on an interconnect of the IBMPG4 benchmark.



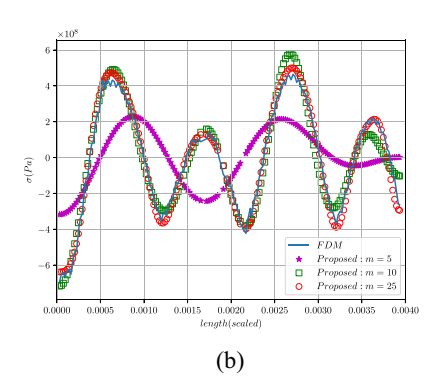


Fig. 13. (a) Steady-state stress  $\sigma(x,\infty)$  and (b) transient stress  $\sigma(x,t)$  on an interconnect of IBMPG4 benchmark are represented by different number of eigenfunctions.

the FDM are both implemented in C++ and tested on a Linux server with  $2 \times 16$  core 3.3-GHz CPU and 128-GB memory. Both methods solve the transient hydrostatic solution for time

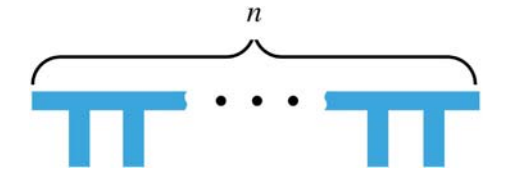


Fig. 14. n T-junctions interconnect structure.

		FDM(sec)				
n	$t_{eig}$	$t_{coef}$	$t_{\sigma}$	$t_{total}$	$t_{all}$	$t_{fdm}$
20	0.099	0.016	0.0076	0.123	0.63	0.32
50	0.152	0.026	0.0094	0.187	1.30	1.61
100	0.485	0.062	0.0180	0.566	2.89	7.20
200	0.960	0.137	0.0358	1.133	5.21	44.5
500	2.372	0.407	0.1356	2.915	14.6	298.4
700	2.406	0.692	0.1632	3.262	17.8	611.5
900	3.171	0.919	0.1926	4.283	23.8	1114.5
1000	5.423	0.832	0.1723	6.428	25.8	1443.9
1200	4.340	1.822	0.2757	6.439	36.8	2080.4
1500	5.856	1.837	0.3442	8.123	44.1	3525.4
1700	6.713	2.242	0.3516	9.307	48.5	5581.6
1900	6.981	2.346	0.3489	9.676	50.3	8053.1
2000	10.53	2.056	0.3579	12.95	51.4	15651.2
10000	49.71	13.83	2.5851	66.13	236.7	NA
50000	231.2	56.86	11.024	299.1	1393.6	NA
100000	441.8	141.7	26.984	610.5	2969.9	NA

 $t=2\times10^7$  s. The proposed method is set to analyze the transient solution with the number of eigenfunctions being 200, which is conservative to ensure sufficient accuracy. For FDM, the interconnect trees are discretized to ten grids per branch spatially and time step  $\Delta t=2\times10^5$  s to run the simulation. For the sake of performance comparison, our method is also set to solve for the stress distribution on the ten grid points on each branch, which is not necessary for practical EM analysis where only stresses on junction nodes are of interest.

In addition, we also tested the time costs of the three major steps of the proposed method: 1) calculate the eigenvalues and eigenfunctions with given boundary conditions; 2) calculate the coefficients of eigenfunctions with given current density and initial stress distribution; and 3) compute the transient hydrostatic solution distribution at time t using the eigenfunctions. In the simulation, the eigenvalues and eigenfunctions need to be calculated only once no matter how many transient hydrostatic stresses to solve. Moreover, as long as the current density distribution remains the same, it is not necessary to calculate the coefficients of eigenfunctions again. As a result, the only repetitive computational cost left is that of computing the transient hydrostatic stress as the linear combination of eigenfunctions, which is significantly cheaper.

Table I shows the time costs of the proposed method and FDM for varying n T-junctions. Here,  $t_{\rm fdm}$  is the time cost of FDM according to above-mentioned discretization schema.  $t_{\rm eig}$ ,  $t_{\rm coef}$ , and  $t_{\sigma}$  are the time costs of the three steps of the proposed method, namely, eigenvalues and eigenfunctions calculation, coefficients calculation, and transient stress calculation, respectively. In addition to the time cost  $t_{\rm total}$  of direct calculation of stress at  $t = 2 \times 10^7$  s, we also present the

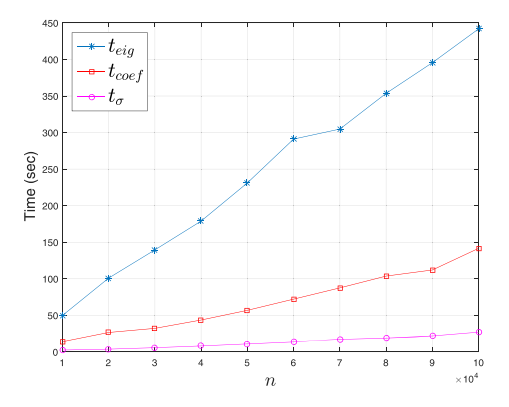


Fig. 15. Histogram of the branch number of IBMPG6.

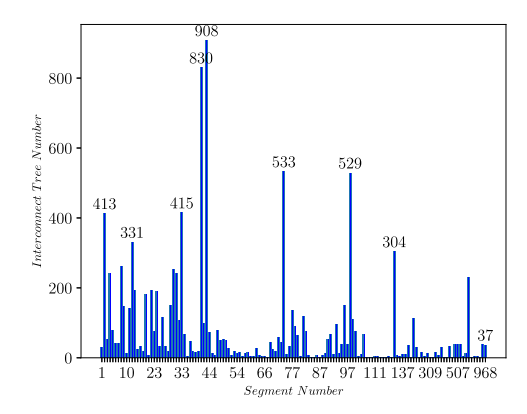


Fig. 16. Time costs of three steps of the proposed method with varying n.

time cost  $t_{\rm all}$  of calculating the transient stresses for all time steps  $\Delta t, 2\Delta t, 3\Delta t, \ldots, 100\Delta t$ . Note that calculating for all time steps is also for the sake of comparison to FDM. In contrast to FDM, our method could just skip the time points at which the hydrostatic stress is irrelevant to EM failure in practical EM analysis. See the next section for more discussion on this. As we can see from Table I, the proposed method is 10X-100X times faster than FDM.

Moreover, the proposed method scales well for larger interconnect trees, which facilitates its practical use for large full-chip networks. Actually, the interconnect trees in practical power/ground networks are not very big because only wires on the same metal layer can form an interconnect tree. Fig. 15 shows the histogram of the branch number of IBMPG6 P/G networks. It could be seen the largest interconnect tree has less than 1000 branches and the majority of the interconnect trees are relatively small ( $\leq 1000$  branches). Therefore, repetitive T-junction trees are intentionally made quite large, with the branch number up to 200 000, to show the scalability of the proposed method. The FDM fails to solve the stress for a huge n larger than 10 000, while the proposed method can handle the large trees with n up to 100 000. Note that only sparse LU factorization of the K matrix is required in the proposed method. Since the sparsity pattern of the K matrix is fully exploited, the proposed method has linear complexity in computing the eigenfunctions by LU factorization. Fig. 16 shows the time costs of the three parts of the proposed method for varying nT-junctions. All the computational costs of three steps increase linearly with the size of the interconnect tree, which means the proposed method scales well for large interconnect trees.

**Algorithm 2:** Bisection Algorithm to Decide the  $t_{\text{nuc}}$  Based on Solution (19)

```
Input: Interconnects T on P/G networks and Korhonen's equations with
        ICs and BCs for these interconnect trees.
Output: Void nucleation time t_{nuc}
Initialize the trial eigenvalue \mu to an arbitrary value \lambda_0;
while N(\mu) < M do
     \mu = 2\mu;
Associate the N(\mu) to interval r_0 = ([0, \mu], 0, N(\mu));
Initialize the intervals to check as queue R = \{r_0\};
while R \neq \emptyset do
     Pop the first interval r from R, i.e. r = pop(R);
     Denote r = ([\mu_b, \mu_e], N(\mu_b), N(\mu_e)) where \mu_b is the start point
        and \mu_e is the end point of interval r;
     if N(\mu_b) > M then
          Drop interval r. Continue;
     else if N(\mu_b) = N(\mu_e) then
          Drop interval r. Continue;
     else if \mu_e - \mu_b < \epsilon then
          for i = N(\mu_b):N(\mu_e) do
               \lambda_i = (\mu_b + \mu_e)/2;
          end
          Finish processing interval r. Continue;
     else
          Calculate N(\mu_m) for middle point \mu_m = (\mu_b + \mu_e)/2 of
          Append both interval r_l = ([\mu_b, \mu_m], N(\mu_b), N(\mu_m)) and
             r_r = ([\mu_m, \mu_e], N(\mu_m), N(\mu_e)) to queue R;
     end
end
```

# D. Analytical Solution-Based Bisection Algorithm for Full-Chip Nucleation Time Determination

Since the proposed method avoids discretization either spatially or temporally, it can skip the calculation of hydrostatic stress on any location or at any time if this stress is irrelevant to the EM failure. In contrast, FDM [12], as well as its accelerated version [15], have to calculate all stress distribution at all time steps because discretized hydrostatic stresses on the interconnect tree are coupled together.

Moreover, the proposed method provides the analytical solution of the hydrostatic stress, although eigenvalues and eigenfunctions have to be determined numerically. Therefore, we can take advantage of the analytical solution to facilitate efficient algorithms. For example, the effective algorithms proposed in [4] to find out the void nucleation time  $t_{\rm nuc}$ , such as the bisection method or Newton's method, could still be utilized with our method, but more accurate since transient hydrostatic stress is provided instead of steady-state stress.

Here, we propose a bisection algorithm (Algorithm 2) based on our semi-analytical solution to decide  $t_{\text{nuc}}$  for P/G networks. Thanks to the proposed closed-form solution (19) of the transient hydrostatic stress, we could determine the void nucleation time  $t_{\text{nuc}}$  for power/ground networks using this equation solving technique instead of checking in a step-by-step manner. Note that the eigenvalues  $\lambda_m$ , eigenfunctions  $\psi_m(x)$ , and coefficients  $C_m$  have to be calculated beforehand to use the solution (19). Since ICs and BCs remain unchanged in the void nucleation phase, it needs to calculate these parameters only once to obtain  $t_{\text{nuc}}$ , which is time efficient.

Table II shows the experimental results of the void nucleation time for full-chip IBMPG benchmarks. Both algorithms are implemented in C++ and tested on a Linux server with  $2 \times 16$  core 3.3-GHz CPU and 128-GB memory. Note the FDM-based algorithm has to check  $t_{\rm nuc}$  in a step-by-step manner

TABLE II
RUNTIME COMPARISON OF THE PROPOSED ALGORITHM 2 AND FDM TO
CALCULATE VOID NUCLEATION TIME

Power Grid			Void N	ucleation Time (yrs)	Runtime (sec)	
Name	#Trees	max #seg	FDM	Proposed	FDM	Proposed
IBMPG2	462	192	0.56	0.56	196	82
IBMPG3	8189	965	4.22	4.20	2191	754
IBMPG4	9641	571	2.88	2.78	1676	581
IBMPG5	1982	281	1.62	1.60	1800	558
IBMPG6	10246	968	6.91	6.96	7054	2081

while the eigenfunction-based algorithm utilizes bisection. The experimental results show that the eigenfunction-based bisection algorithm is about three (2.96) times faster than FDM on average. In Table II, "#Trees" is the number of interconnect trees and "max #seg" is the maximum branch number of interconnect trees. Although the number of interconnect trees is large in these benchmarks, the size of the interconnect tree (i.e., the number of branches) is relatively small. This makes the speedup in this experiment is not as significant as those shown in Table I. Nevertheless, the benefits of the proposed analytical solution are still demonstrated by the experiment results.

#### VII. CONCLUSION

In this article, an accurate transient analysis method is proposed for the hydrostatic stress evolution on general 2-D multibranch interconnect trees to facilitate fast full-chip EM assessment. The proposed method is based on the technique of eigenfunction and could solve Korhonen's equation for multibranch interconnect trees stressed with different current densities and nonuniformly distributed thermal effects. The proposed method can also accommodate the pre-existing residual stresses coming from thermal or other stress sources. The proposed method is consistent with the previous analytical solutions for a single wire and 1-D multisegment wires. The transient hydrostatic stress evolution could be calculated accurately by the proposed method so that the void nucleation could be simulated precisely. Our numerical results show that the proposed method is 10X-100X faster than the finite difference method and scales better for larger interconnect trees. The benefits of the analytical solution also make the proposed method more friendly to EM optimization than numerical methods.

In future work, the proposed method would be extended to accommodate the time-varying current densities and thermal effect. In addition, more irregular shapes and impacts due to lithography can be a topic for future investigation.

#### REFERENCES

- J. Black, "Electromigration—A brief survey and some recent results," *IEEE Trans. Electron Devices*, vol. ED-16, no. 4, pp. 338–347, Apr. 1969.
- [2] I. A. Blech, "Electromigration in thin aluminum films on titanium nitride," J. Appl. Phys., vol. 47, no. 4, pp. 1203–1208, Apr. 1976.
- [3] M. Hauschildt et al., "Electromigration early failure void nucleation and growth phenomena in Cu and Cu(Mn) interconnects," in Proc. IEEE Int. Rel. Phys. Symp. (IRPS), Apr. 2013, pp. 1–6.
- [4] X. Huang, A. Kteyan, S. X.-D. Tan, and V. Sukharev, "Physics-based electromigration models and full-chip assessment for power grid networks," *IEEE Trans. Comput.-Aided Design Integr. Circuits Syst.*, vol. 35, no. 11, pp. 1848–1861, Nov. 2016.

- [5] M. Pathak, J. Pak, D. Z. Pan, and S. K. Lim, "Electromigration modeling and full-chip reliability analysis for BEOL interconnect in TSV-based 3D ICs," in *Proc. IEEE/ACM Int. Conf. Comput.-Aided Design (ICCAD)*, Nov. 2011, pp. 555–562.
- [6] V. Sukharev, X. Huang, H.-B. Chen, and S. X.-D. Tan, "IR-drop based electromigration assessment: Parametric failure chip-scale analysis," in *Proc. IEEE/ACM Int. Conf. Comput.-Aided Design (ICCAD)*, Nov. 2014, pp. 428–433.
- [7] S. Chatterjee, V. Sukharev, and F. N. Najm, "Fast physics-based electromigration checking for on-die power grids," in *Proc. 35th Int. Conf. Comput.-Aided Design (ICCAD)*, 2016, pp. 1–8.
- [8] M. A. Korhonen, P. Borgesen, K. N. Tu, and C.-Y. Li, "Stress evolution due to electromigration in confined metal lines," *J. Appl. Phys.*, vol. 73, no. 8, p. 3790, Apr. 1993.
- [9] H.-B. Chen, S. X. Tan, X. Huang, T. Kim, and V. Sukharev, "Analytical modeling and characterization of electromigration effects for multi-branch interconnect trees," *IEEE Trans. Comput.-Aided Design Integr. Circuits Syst.*, vol. 36, no. 11, pp. 1811–1824, Nov. 2016.
- [10] H.-B. Chen, S. X.-D. Tan, J. Peng, T. Kim, and J. Chen, "Analytical modeling of electromigration failure for VLSI interconnect tree considering temperature and segment length effects," *IEEE Trans. Device Mater. Rel.*, vol. 17, no. 4, pp. 653–666, Dec. 2017.
- [11] X. Wang, H. Wang, J. He, S. X.-D. Tan, Y. Cai, and S. Yang, "Physical-based electromigration modeling and assessment for multi-segment interconnects in power grid networks," in *Proc. Design Autom. Test Europe Conf.*, 2017, pp. 1727–1732.
- [12] C. Cook, Z. Sun, T. Kim, and S. X. D. Tan, "Finite difference method for electromigration analysis of multi-branch interconnects," in *Proc. 13th Int. Conf. Synth. Model. Anal. Simulat. Methods Appl. Circuit Design* (SMACD), 2016, pp. 1–4.
- [13] S. Chatterjee, V. Sukharev, and F. N. Najm, "Power grid electromigration checking using physics-based models," *IEEE Trans. Comput.-Aided Design Integr. Circuits Syst.*, vol. 37, no. 7, pp. 1317–1330, Jul. 2018.
- [14] S. Chatterjee, V. Sukharev, and F. N. Najm, "Fast physics-based electromigration assessment by efficient solution of linear time-invariant (LTI) systems," in *Proc. IEEE/ACM Int. Conf. Comput.-Aided Design (ICCAD)*, Nov. 2017, pp. 659–666.
- [15] C. Cook, Z. Sun, E. Demircan, M. D. Shroff, and S. X.-D. Tan, "Fast electromigration stress evolution analysis for interconnect trees using Krylov subspace method," *IEEE Trans. Very Large Scale Integr. Syst.*, vol. 26, no. 5, pp. 969–980, May 2018.
- [16] X. Wang, Y. Yan, J. He, S. X.-D. Tan, C. Cook, and S. Yang, "Fast physics-based electromigration analysis for multi-branch interconnect trees," in *Proc. IEEE/ACM Int. Conf. Comput.-Aided Design (ICCAD)*, Nov. 2017, pp. 169–176.
- [17] V. Sukharev, A. Kteyan, E. Zschech, and W. Nix, "Microstructure effect on EM-induced degradations in dual inlaid copper interconnects," *IEEE Trans. Device Mater. Rel.*, vol. 9, no. 1, pp. 87–97, Mar. 2009.
- [18] B. Li, C. Christiansen, D. Badami, and C.-C. Yang, "Electromigration challenges for advanced on-chip Cu interconnects," *Microelectron. Rel.*, vol. 54, no. 4, pp. 712–724, 2014.
- [19] Z. Sun, E. Demircan, M. D. Shroff, C. Cook, and S. X.-D. Tan, "Fast electromigration immortality analysis for multi-segment copper interconnect wires," *IEEE Trans. Comput.-Aided Design Integr. Circuits* Syst., vol. 37, no. 12, pp. 3137–3150, Dec. 2018.
- [20] W. H. Wittrick and F. W. Williams, "A general algorithm for computing natural frequencies of elastic structures," *Quart. J. Mech. Appl. Math.*, vol. 24, no. 3, pp. 263–284, 1971.
- [21] A. George and J. W. H. Liu, Computer Solution of Large Sparse Positive Definite Systems (Computational Mathematics). Englewood Cliffs, NJ, USA: Prentice-Hall, 1981.
- [22] L. V. Foster and T. A. Davis, "Algorithm 933: Reliable calculation of numerical rank, null space bases, pseudoinverse solutions, and basic solutions using SuitesparseQR," ACM Trans. Math. Softw., vol. 40, no. 1, pp. 1–23, 2013.
- [23] J. Miao, M. Li, S. Roy, Y. Ma, and B. Yu, "SD-PUF: Spliced digital physical unclonable function," *IEEE Trans. Comput.-Aided Design Integr. Circuits Syst.*, vol. 37, no. 5, pp. 927–940, May 2018.
- [24] S. Nassif, "Power grid analysis benchmarks," in *Proc. Asia South Pac. Design Autom. Conf.*, 2008, pp. 376–381.



**Xiaoyi Wang** received the B.S. and Ph.D. degrees in computer science from Tsinghua University, Beijing, China, in 2004 and 2010, respectively.

In 2014, he joined Beijing University of Technology, Beijing, where he is currently an Associate Professor with the School of Software Engineering. From 2010 to 2014, he was a Senior Engineer with the China Railway Communication and Signalling Research and Design Institute, Beijing. His current research interests include modeling and simulation of on-chip power supply

networks, electromigration modeling and optimization for VLSI, numerical algorithms, and Internet of Things.



**Shaobin Ma** was born in 1996. He received the B.E. degree in geological engineering from the China University of Mining and Technology, Xuzhou, China, in 2017. He is currently pursuing the M.S. degree in software engineering with the Beijing University of Technology, Beijing, China.

His current research interests include electromigration modeling and analysis.



**Sheldon X.-D. Tan** (Senior Member, IEEE) received the B.S. and M.S. degrees in electrical engineering from Fudan University, Shanghai, China, in 1992 and 1995, respectively, and the Ph.D. degree in electrical and computer engineering from the University of Iowa, Iowa City, IA, USA, in 1999.

He is a Professor with the Department of Electrical Engineering, University of California at Riverside, Riverside, CA, USA, where he is also a Cooperative Faculty Member with the Department of Computer Science and Engineering. He has pub-

lished more than 300 technical papers and has coauthored 6 books on the above areas. His recent research interests include machine learning approaches for VLSI reliability modeling, optimization and management at circuit and system levels, learning-based thermal modeling, optimization and dynamic thermal management for many-core processors, parallel computing, and quantum and Ising computing based on GPU and multicore systems.

Prof. Tan received the NSF CAREER Award in 2004. He also received three Best Paper Awards from ICSICT'18, ASICON'17, ICCD'07, and DAC'09. He also received the Honorable Mention Best Paper Award from SMACD'18. He was a Visiting Professor of Kyoto University as a JSPS Fellow from December 2017 to January 2018. He is serving as the TPC Chair of ASPDAC 2021. He also served as the TPC Vice Chair of ASPDAC 2020. He is serving or served as an Editor-In-Chief for Integration, VLSI Journal (Elsevier's), the Associate Editor for three journals: IEEE TRANSACTIONS ON VERY LARGE SCALE INTEGRATION (VLSI) SYSTEMS, the ACM Transaction on Design Automation of Electronic Systems, and Microelectronics Reliability (Elsevier's).



Chase Cook (Graduate Student Member, IEEE) received the B.S. degree in computer engineering from California State University at Bakersfield, Bakersfield, CA, USA, in 2015, and the Ph.D. degree in electrical and computer engineering from the University of California at Riverside, Riverside, CA, USA, in 2019.

His current research interests include electronic design automation and simulation of aging effects in integrated circuits.

**Liang Chen** (Student Member, IEEE), photograph and biography not available at the time of publication.

**Jianlei Yang** (Member, IEEE), photograph and biography not available at the time of publication.

Wenjian Yu (Senior Member, IEEE), photograph and biography not available at the time of publication.